Supplementary Information

Efficient and Stable Electrochemical Carbon Capture via Integrated CO_2 Absorption and Regeneration

Zhiwei Fang, Junwei Zhang, Peng Zhu, Zhou Yu, Ahmad Elgazzar, Juan Wang, Wei Ping Lam, and Haotian Wang

Table of Contents:

Supplementary Methods

Three-chamber PSE cell configuration and electrochemical measurement:

The salt splitting and acid/base generation were conducted in a porous solid electrolyte (PSE) cell. The cell configurations and operating procedures are illustrated in **Fig. 2b and c**. The cation exchange membranes (CEM) close to the cathode (cathodic ORR catalysts: Pt/C or Co-SAC on hydrophobic carbon cloth electrode) is Nafion N2100TX or ePTFE reinforced Nafion membrane, and the proton exchange membrane (PEM) close to the anode side (anodic OER catalysts on carbon paper, IrO_x or RuO_x on gas diffusion layer electrode) is the Nafion-117 membrane. The active electrode area was 4.0 or 1.0 cm^2 in this study. In the middle chamber, Diaion (Na) ion exchange resin was employed as the PSE.[1,2] The flow rate at the outlet was calibrated using a measuring cylinder. The cathode side was provided with a mixture of gas of different concentrations of O_2 and CO_2 or atmosphere for ORR and CO_2 capture reaction. All cell resistances were measured by the potentiostatic electrochemical impedance spectroscopy (PEIS), and all the cell voltages in our work were reported **without** any iR compensation. For the flue gas capture, a simulated flue gas (CO_2, O_2 or atmosphere air) was prepared as the gas input to the reactor system. All gas flow rates were precisely controlled by the mass flow controllers and the concentration of the mixture was measured and recorded by a CO_2 meter (sensor from CO2Meter).[3,4] Flow rates of 50 sccm were used for simulated flue gas or pure oxygen, and 1000 sccm for direct air capture experiments. The middle solid-electrolyte layer was continuously flowed with 1.0 ml min^{-1} of (bi)carbonate electrolyte, and the cathode side was circulated with 1.0 ml h^{-1} of electrolyte.

Synthesis of SACs

The method used for synthesizing Co-SAC is based on our previously reported method, with some modifications.[5] First, 1.0 g of *o*-phenylenediamine, 0.44 g of $CoCl_2$, and 2.0 g of SiO_2 nanoparticles (10–20 nm, Aldrich) templates were mixed together by using 20 ml 1.0 M HCl solution. Then, the mixed solution was sonicated for 0.5 h and stirred for another 0.5 h. Subsequently, 12 ml of 1.0 M HCl solution, which contains 3.0 g of ammonium peroxydisulfate, that is, $(NH_4)_2S_2O_8$, was added dropwise into the above-mixed solution with vigorous stirring. After polymerization in an ice bath for nearly one day, the mixture was dried using a rotary evaporator. Then, the dried powder was annealed under Ar atmosphere at 800 °C for 2 h. Finally,

the product was treated by alkaline (2.0 M NaOH) and acid (2.0 M H_2SO_4) leaching successively to remove SiO_2 nanoparticles templates and unstable Co-based species, respectively, to obtain the Co-SAC. We used the same method to prepare Ni-SAC. The only difference is that 0.405 g $NiCl_2 \cdot 6H_2O$ and 1.0 g SiO_2 were used to synthesize Ni-SAC. Fe-SAC was obtained on the basis of our previous paper.

Preparation of electrode

For the preparation of the cathode electrode, 40 mg of as-prepared single-atom catalysts, 4 ml of 2-propanol (Sigma-Aldrich), and 160 µl of Nafion binder solution (Sigma, 5%) were mixed together to form a catalyst ink with around 10.0 mg ml^{-1}. The ink was sonicated for about 30 min to obtain a homogeneous ink and then spray coated onto the 5 × 5 cm^2 CT Carbon Cloth with MPL (carbon cloth; Fuel Cell Store) electrodes. The Pt/C (Fuel Cell Store) used in this work followed the same procedure to prepare the cathode electrode. IrO_x and RuO_x electrodes purchased from Dioxide Materials were used for the anode electrodes during the electrochemical process.

Gas analysis

Water-displacement measurement was used to measure the gaseous CO_2 flow rate at the outlet of middle chamber.[4,6] To minimize gas dissolution, CO_2-saturated 0.01 M H_2SO_4 was used during the measurement. It was pre-saturated with CO_2 to minimize the gas dissolution and the acid was used to further suppress CO_2 solubility during the bubble flow rate analysis. The captured CO_2 from catholyte was quantified using titration with 0.1 M HCl and a pH meter (Orion Star A111). Gas chromatography with TCD and FID detection was used to analyze O_2 and N_2 impurities in the produced CO_2.

Contour map generation

To visualize the spatial variation of CO_2 concentration and currents for captured CO_2 species distribution (**Fig. 4e**) and sorbent utilization efficiency (**Fig. 4f**), contour maps were generated using experimental data. For non-uniformly spaced points, Shepard interpolation was applied via the XYZ gridding tool to produce a regular Z matrix. The data were then plotted using the *Contour - Color Fill* option, with color scales and levels adjusted to emphasize the distribution of captured CO_2 species and the orbital utilization efficiency.

Definition & Calculations:

Ion transport number calculation

t: Cation transport number (or cation transport efficiency, between 0 and 1) describes the number of cations crossed through CEM over the total number of electrons transferred.

t_{Na^+} : Na^+ transport number (or Na^+ transport efficiency) describes the amount of Na^+ crossed through CEM over the total number of electrons transferred. The concentration of Na^+ was determined *via* ion chromatography (IC) and inductively coupled plasma mass spectrometry (ICP-MS) characterization. For continuous flow, the *t* for Na^+ at the cathode is calculated using the following equation:

$$t_{Na^+} = \frac{Na^+ \left(mol\ L^{-1}\right) \times 96485 \left(C\ mol^{-1}\right) \times flow\ rate\ (mL\ s^{-1})}{60 \times j_{total}\ (mA)} \times 100$$

For recirculation flow, the *t* for Na^+ at the cathode is calculated using the following equation:

$$t_{Na^+} = \frac{Na^+ \left(mol\ L^{-1}\right) \times volume\ (L)}{j_{total}\ (A) \times time\ (s)/96485\ (C\ mol^{-1})} \times 100$$

Energy consumption is calculated using the following equation:[4,6]

$$Energy\ consumption\ (kJ/mol) = \frac{power\ input}{CO_2\ capture\ rate} = \frac{voltage\ (V) \times Current\ density}{\frac{Current\ density \times FE}{n \times 96485\ C/mol}} \times \frac{1kJ}{1000J} = \frac{n \times voltage \times 96485}{EE \times 1000}$$

Cell voltage breakdown analysis

For an ideal electrochemical cell used for pH swinging, the thermodynamic limit of the total cell voltage can be expressed as:[26]

$$VCell,ideal = \frac{2.303 \times RT}{F}\left(pH_{basified} - pH_{acidified}\right) \quad (1)$$

Where *R* is the universal gas constant (8.3144 J K^{-1} mol^{-1}), *T* is the temperature, *F* is the Faraday constant (9.6485 × 10^4 C mol^{-1}). This equation, derived from the Nernst equation, accounts for the

pH gradient across the cell. The term $pH_{basified}$ refers to the pH at the cathode interface in the basified compartment, while $pH_{acidified}$ represents the pH at the anode interface in the acidified compartment.

The practical cell voltage ($V_{cell,\ practical}$) can be expressed as the following equation:

$$VCell,practical = \frac{2.303 \times RT}{F}\left(pH_{basified} - pH_{acidified}\right) + V_{rxn,\ overpotential} + iR$$

$$= \frac{2.303 \times RT}{F}\left(pH_{cathode} - pH_{anode}\right) + VOER,\ overpotential + VORR,\ overpotential$$

$$+ iRPSE + iRmembrane + iRelectrode$$

(2)

This equation incorporates three main contributing factors: (1) pH overpotential, (2) catalyst overpotentials for the anodic and cathodic half-reactions (activation energy barriers), and (3) the internal resistance (ohmic drop) of the cell. In this study, $V_{rxn,\ overpotential}$ refers to the overpotentials of anodic OER and cathodic ORR catalysts, while the cell resistance (iR), includes PSE resistance, membrane resistance, and electrode resistance.

Technoeconomic Analysis of Gas Separation

For 2-chamber PSE electrolysis, the anode-PSE chamber outlet gas consists of CO_2 and O_2 with a varying volume ratio, depending on the sorbent utilization efficiency and CO_2 concentration. Herein, we analyzed the operation cost and capital cost for the separation of CO_2 and O_2 with a 1:1 volume ratio. For gas product separation, pressure swing adsorption (PSA) is an industrially used process with low operating cost and high efficiency. All the assumptions and models in our TEA were based on previous literature.[7] PSA reference cost is \$1989043, PSA operating cost is 0.3 kWh/m^3.

1. Total Separation Cost

$$Final\ separation\ cost = \frac{PSA\ capital\ cost}{20\ years \times \frac{350days}{year} \times 24\ h/day} + PSA\ operating\ cost\ per\ hour$$

The final separation cost per hour is calculated as the sum of the amortized capital cost and the operating cost. Assuming a production of 1000kg/h, Electricity Price is 0.03 $/kWh, CO_2 : O_2 is 1:1 with 554.54 m^3/h, total outlet flow is 1109.1 m^3/h

$$PSA\ capital\ cost = \$1989043 \times 1109.1/1000 = \$2142827$$

$$PSA\ operating\ cost\ per\ hour = 0.3kWh/m^3 \times 1109.1\ m^3/h \times 0.03\ \$/kWh = \$9.982/h$$

Thus, PSA operating cost per hour = \$2142827/(20×350×24)/h + \$9.982/h

Final separation cost = \$12.75/h + \$9.982/h = \$22.74/h

2. Final Energy Consumption

This cost is then converted to an equivalent energy consumption using the assumed electricity price 0.03 $/kWh

$$Final\ energy\ consumption = Final\ separation\ cost / Electricity\ Price$$

$$Final\ energy\ consumption = \$22.74/h / \$0.03kWh = 757.9\ kW$$

This \$757.9 kW represents the separation power required for the PSA separation process for a CO_2 regeneration rate of \$1000 kg/h

$$Total\ current = 1000kg/h \times h/3600s \times kmol/44kg \times n \times 96485\ C/mol$$

The current is 1,218,244.9A if captured as carbonates and 609,122.45A if captured as bicarbonates.

The power needed is given by P = UI. The final energy consumption is 757.9 kW, so it could tolerate ~ 621.6 mV if captured as carbonates and 1.22 V if bicarbonates. Assuming EE is 90%,

$$Energy\ consumption\ (kJ/mol) = \frac{voltage\ (V)\ \times Current\ density}{\frac{Current\ density\ \times\ FE}{n\ \times 96485\ C/mol}} \times \frac{1kJ}{1000J} = \frac{n\ \times\ voltage\ \times 96485}{EE\ \times 1000} = 133kJ/mol$$

Based on our calculation, when the additional energy consumption associated with the 3-chamber PSE is lower than 130 kJ/mol, the overall cost of using the 3-chamber PSE for in situ pure CO_2 regeneration becomes lower than the cost of performing CO_2-O_2 separation via PSA. As shown in **Fig. 5c**, the difference in energy consumption between the 2-chamber PSE and the 3-chamber PSE is consistently below this 130 kJ/mol threshold, demonstrating the economic advantage of the 3-chamber configuration for high-purity CO_2 production.

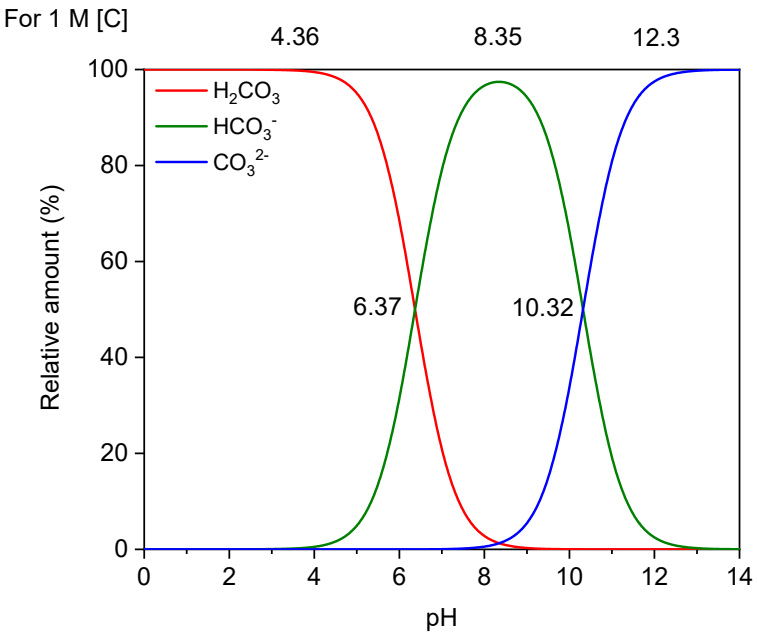

Supplementary Fig. 1. Diagram of carbonate species distribution according to the pH:
Define Z as: $Z = (H^+)^2+(H^+)K_{H2CO3} + K_{H2CO3}\,K_{HCO3}$ or more generally as: $Z = (H^+)^2 + (H^+)K_1 + K_1\,K_2$, where K_1 and K_2 are the first and second dissociation constants for the acid. [8]
K_1 = 6.37 (H_2CO_3), K_2 = 10.32 ($NaHCO_3$), then:

$$\frac{[\,H_2CO_3\,]}{C_T} = \frac{[\,H^+\,]^2}{Z}$$

$$\frac{[HCO_3^-]}{C_T} = \frac{[H^+]\,K_1}{Z}$$

$$\frac{[H_2CO_3]}{C_T} = \frac{K_1\,K_2}{Z}$$

C_T is the sum of all carbonate species concentration, activity coefficients are neglected or equal to one. K_3=~15 (NaOH).

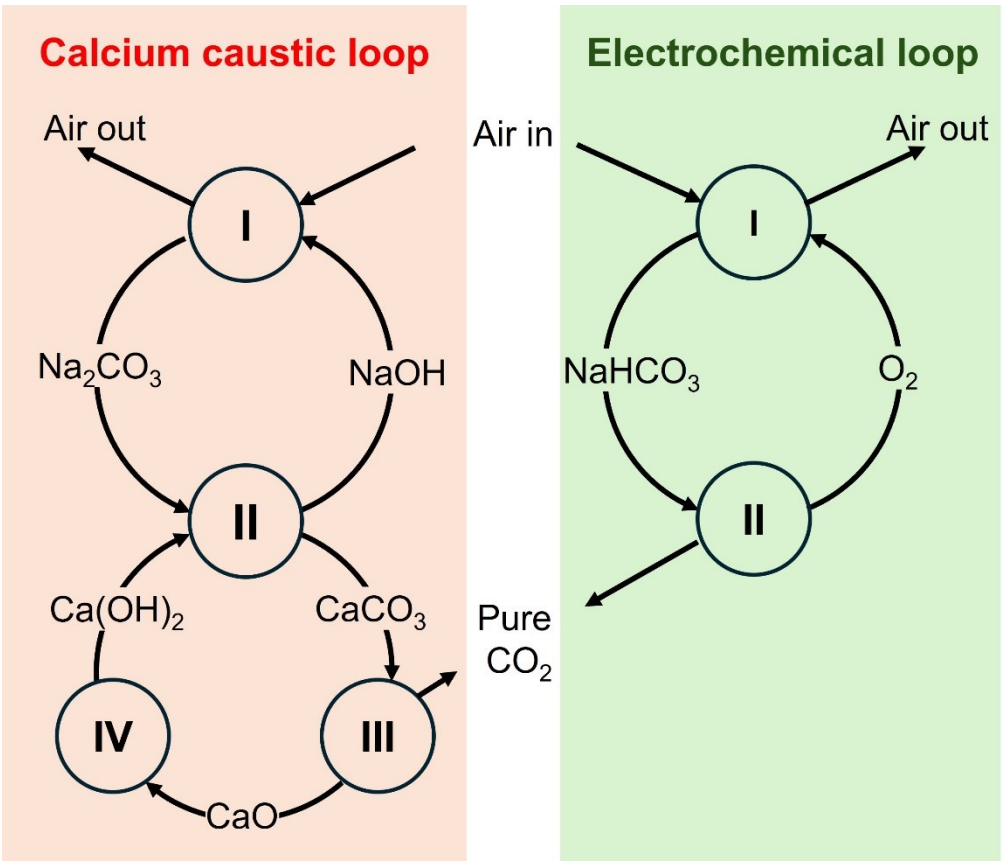

Supplementary Fig. 2. Schematic process of electrochemical CO_2 capture and regeneration loop from flue gas or air in our solid electrolyte reactor.

I: Air contactor: $CO_2(g) + 2NaOH(aq) \rightarrow H_2O(l) + Na_2CO_3\ (aq)$

II: $Na_2CO_3(aq) + Ca(OH)_2(s) \rightarrow 2NaOH(aq) + CaCO_3(s)$

III: CO_2 regeneration: $CaCO_3(s) \rightarrow CaO(s) + CO_2\ (g)$

IV: $CaO(s) + H_2O(l) \rightarrow Ca(OH)_2(s)$

I: Air contactor (Cathode):

$$CO_2 + \frac{1}{4} O_2 + \frac{1}{2} H_2O + e^- \rightarrow HCO_3^-$$

II. CO2 regeneration (Anode & middle chamber):

$$HCO_3^- - e^- \rightarrow \frac{1}{4} O_2 + CO_2 + \frac{1}{2} H_2O$$

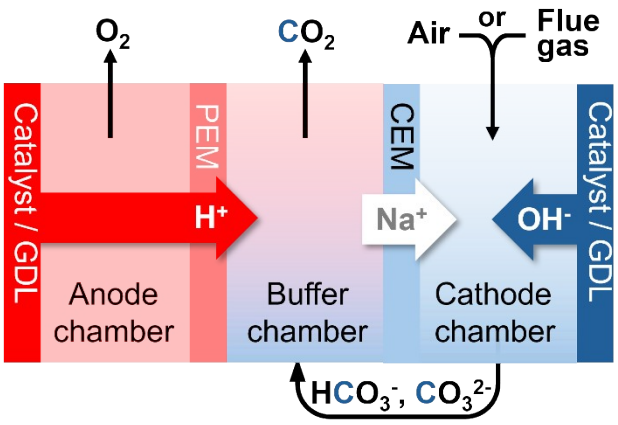

Supplementary Fig. 3. Scheme of the electrochemical carbon absorption and CO_2/sorbent regeneration process from direct air capture or flue gas capture.

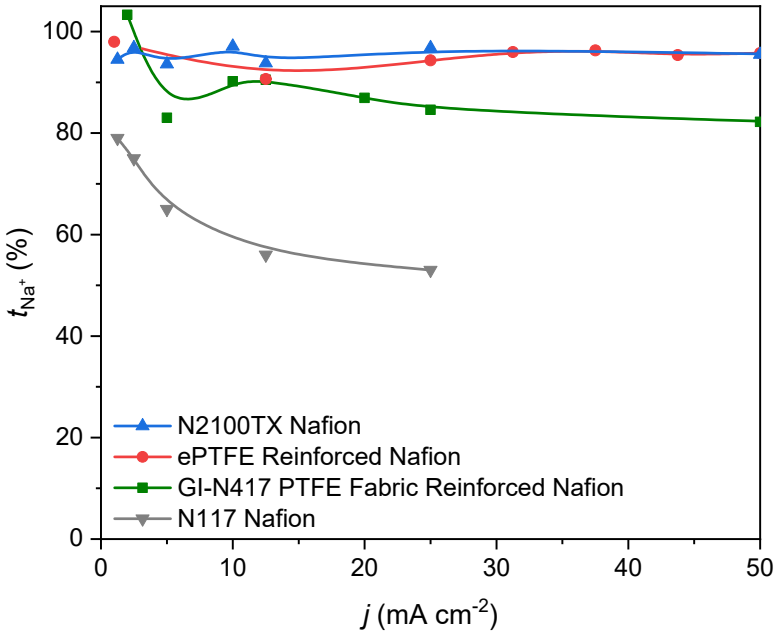

Supplementary Fig. 4. Transport number (t_{Na+}) of different CEMs for sodium transports from the middle buffer chamber to the cathode chamber.

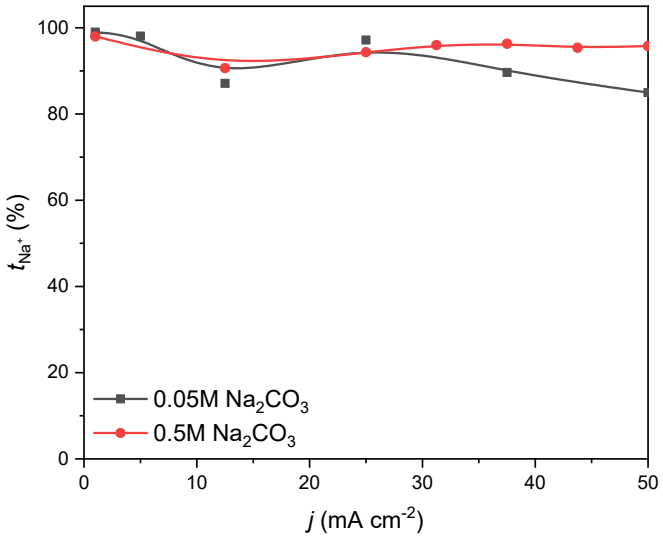

Supplementary Fig. 5. Transport number (t_{Na+}) at lower Na^+ concentration: t_{Na+} of CEM (ePTFE-Nafion) at the Na_2CO_3 concentration of 0.5M and 0.05 M (R.T., 10% CO_2).

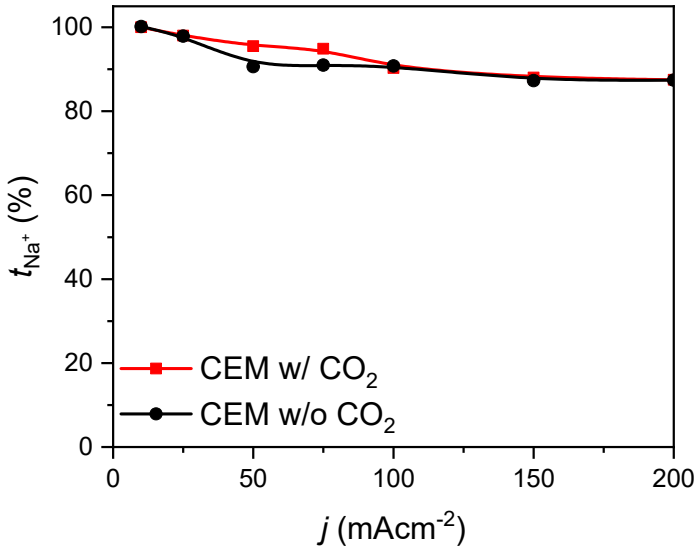

Supplementary Fig. 6. CO_2 effect on t_{Na+} of CEM: t_{Na+} of CEM (ePTFE-Nafion) when the cathodic feeding gas is pure O_2 or 10% CO_2-90% O_2 (R.T., 1.0 M Na^+). The presence of CO_2 at the cathode not only lowers the cell voltage but also slightly enhances higher Na^+ transport efficiency and electrolyzer kinetics, probably due to reduced proton crossover at the lower pH introduced by CO_2 (less proton concentration gradient across the membrane. This effect is even more significant when using a PEM, where proton crossover is typically stronger (**Supplementary Fig. 7**).

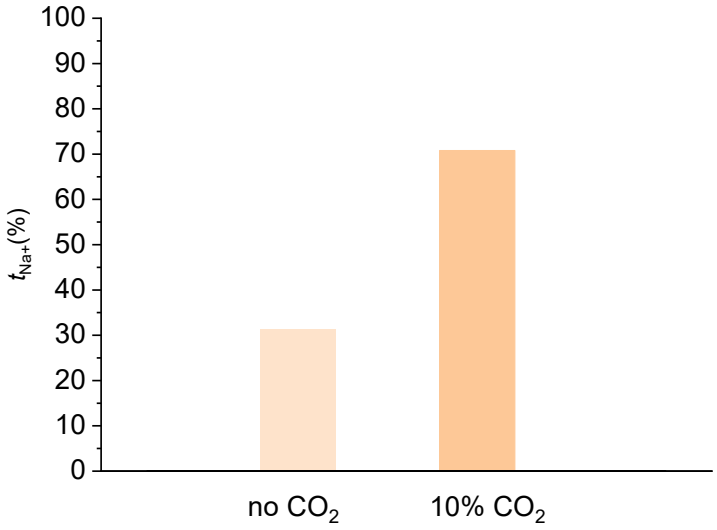

Supplementary Fig. 7. CO_2 effect on t_{Na+} on Nafion1177: t_{Na+} of PEM (Nafion-117) when the cathodic feeding gas is pure O_2 or 10%CO_2-90%O_2 (10mA cm^{-2}, R.T., 1.0 M Na^+).

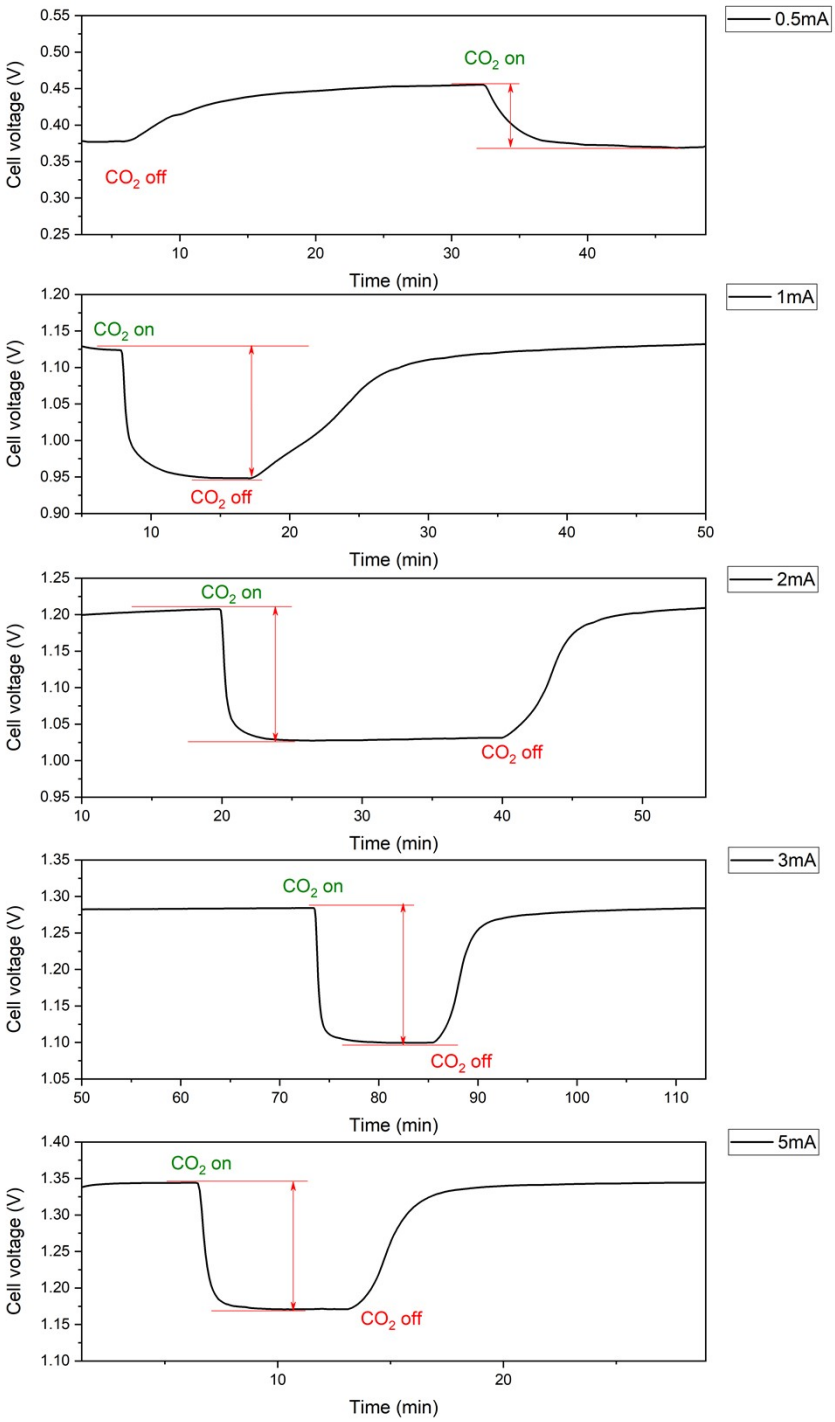

Supplementary Fig. 8. CO_2 effect of cell voltage at the low current.

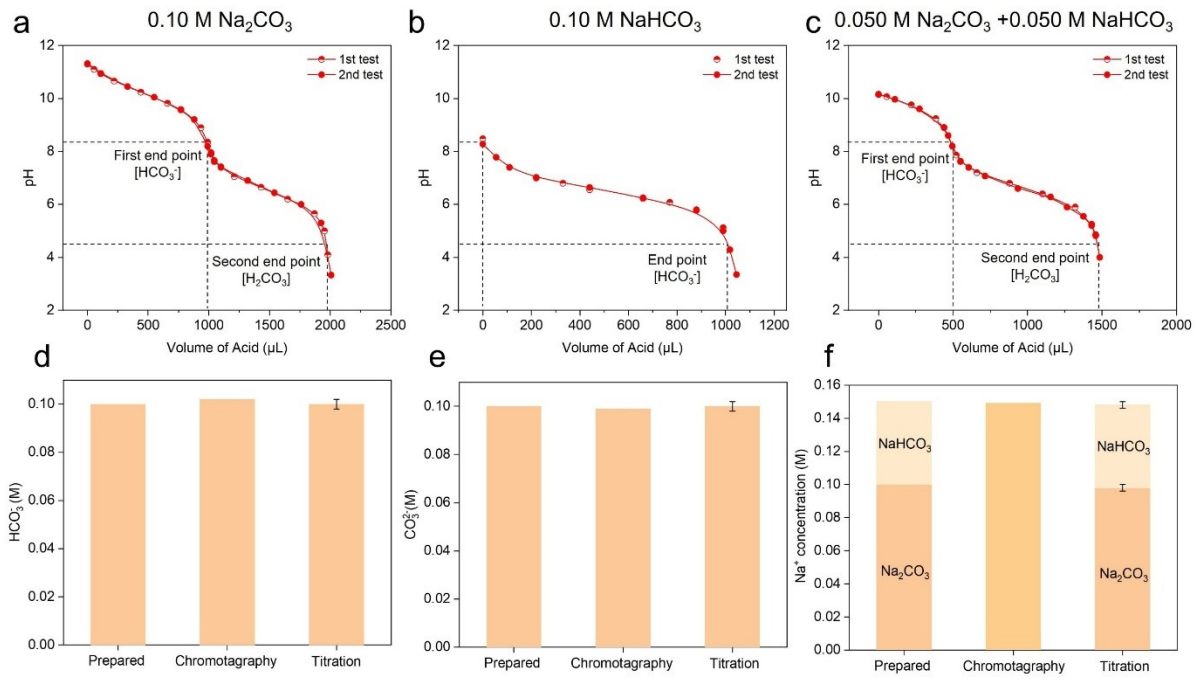

Supplementary Fig. 9. Validation of titration accuracy: To confirm the accuracy of our titration measurement of dissolved CO_2, we prepared 0.10 M Na_2CO_3, 0.10 M $NaHCO_3$, and a 1:1 mixed solution of $NaHCO_3$ and Na_2CO_3 standard solutions. (a, b, c) Titration curve to test the accuracy of the titration method for (a) 0.10 M Na_2CO_3, (b) 0.10 M $NaHCO_3$, and (c) a 1:1 mixed solution of $NaHCO_3$ and Na_2CO_3 standard solutions quantification. The titration was conducted using a 0.1M HCl solution. The first end point is where HCO_3^- predominates, while H_2CO_3 predominates at the second end point. The difference between these two points allows us to estimate the concentration of CO_3^{2-} and HCO_3^-. (d, e, f) Comparison between prepared concentration, ionic chromatography test (based on cation detection), and titrated value of different concentrations. The concentration for prepared and measured results indicated the accuracy and <5% error of our method.

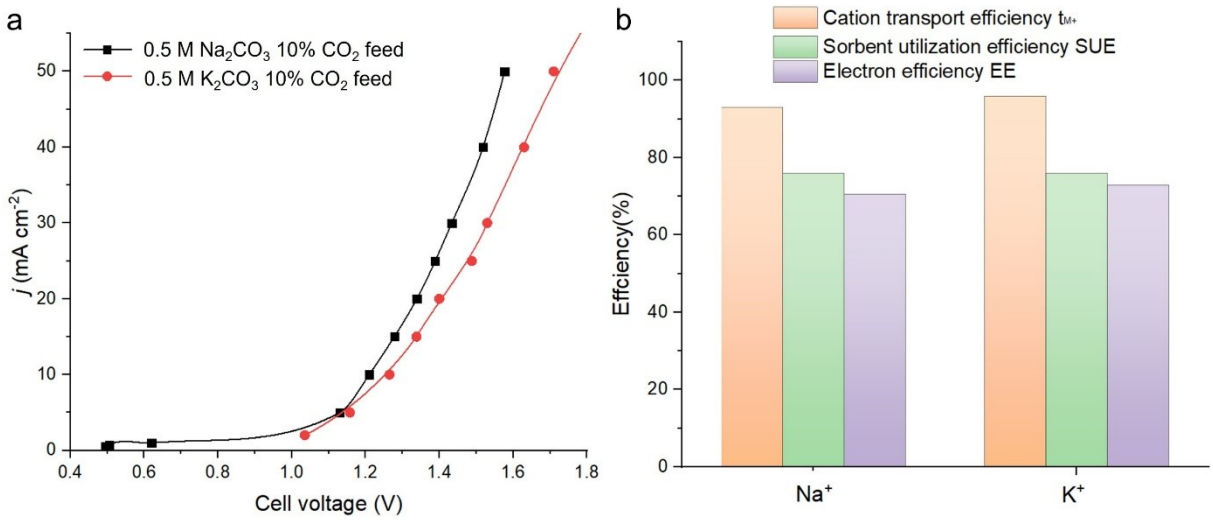

Supplementary Fig. 10. Cation effect: Na^+ vs. K^+: cell voltage and efficiency: When K^+ is used instead of Na^+, the cell voltage is slightly higher, which possibly arises from the higher mobility of Na^+. In terms of efficiency, the measured cation transport efficiency (t_{M+}) and resulting electron efficiency remain similar between Na^+ and K^+, with K^+ showing a slightly higher transport efficiency.

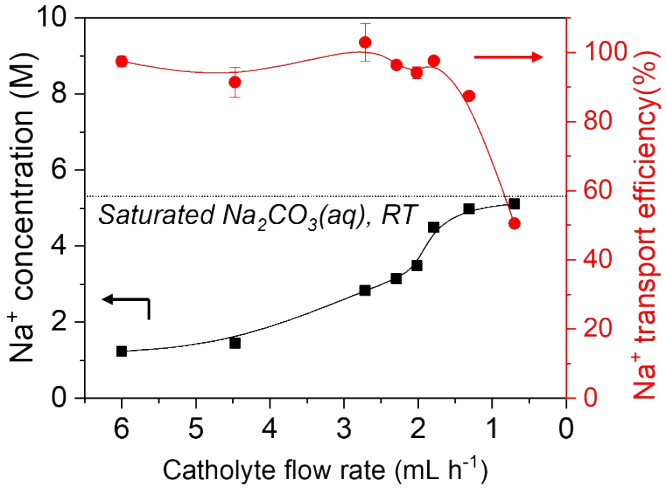

Supplementary Fig. 11. Correlation between Na^+ concentration and catholyte flow rate, along with Na^+ transport efficiency (t_{Na^+}) across the CEM. The system can achieve near-saturated Na_2CO_3 production while maintaining over 80% cation transport efficiency.

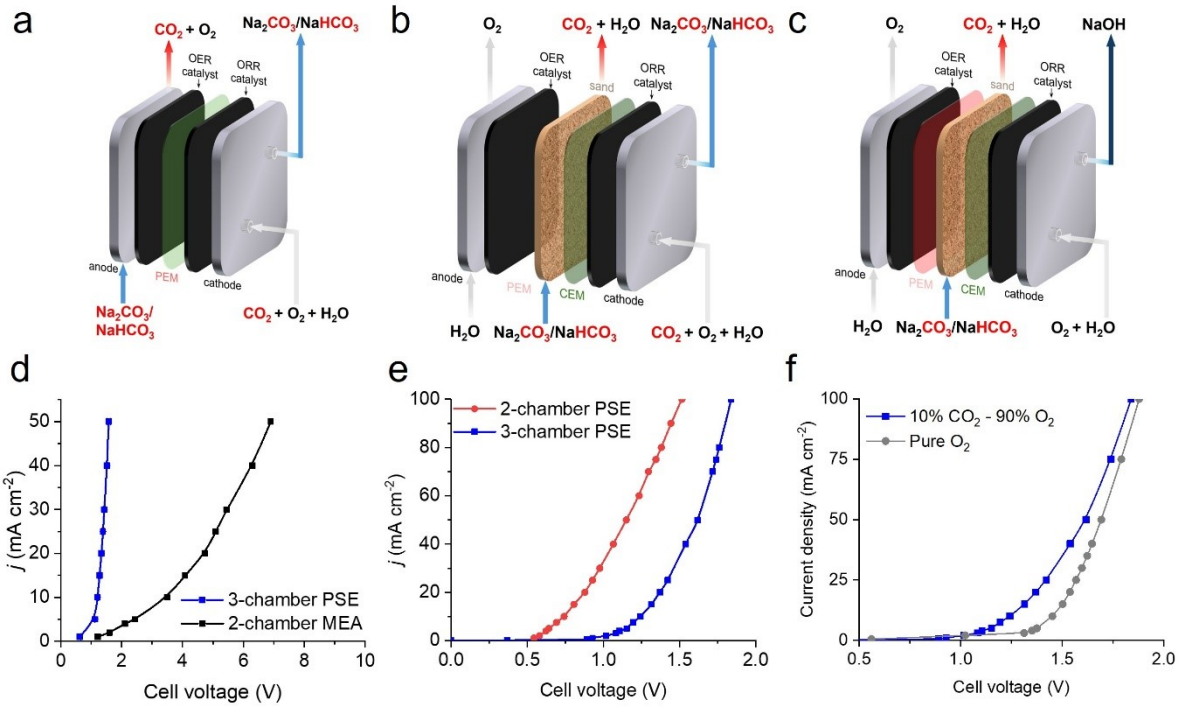

Supplementary Fig. 12. Comparison of our PSE electrolyzer design and performance with other electrochemical reactors featuring different configurations or operation, including: (a) 2-chamber MEA with CO_2 feed., (b) 2-chamber PSE with CO_2 feed., (c) 3-chamber PSE without CO_2 co-feed, and (d)-(f) I-V curves comparing 3-chamber PSE cells with CO_2 feed.

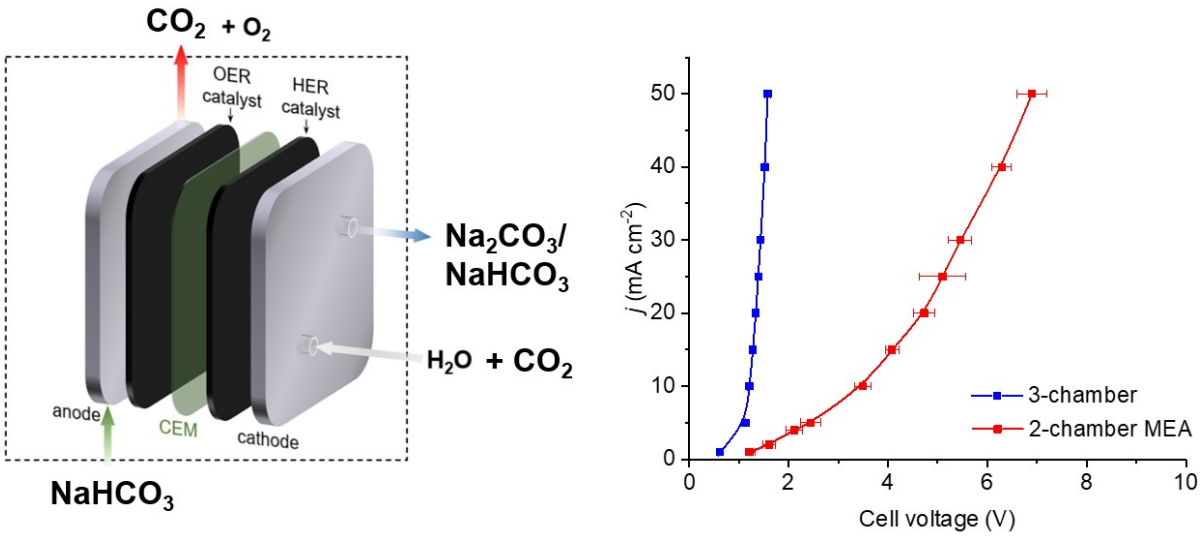

Supplementary Fig. 13. Electrochemical devices for carbon capture and pure CO_2 regeneration using 2-chamber MEA and its i-V curves compared with 3-chamber PSE cells.

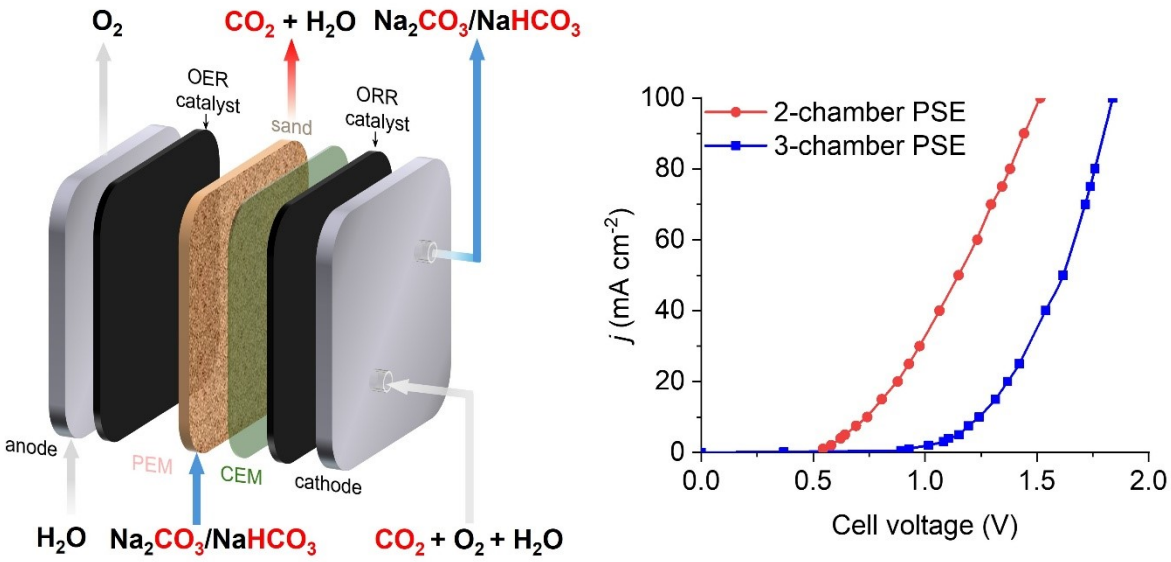

Supplementary Fig. 14. Electrochemical devices for carbon capture and pure CO_2 regeneration using a 2-chamber electrolyzer configuration (no PEM at the anode) and its i-V curves compared with 3-chamber PSE cells. The two-chamber design exhibits a lower cell voltage, likely due to the increased pH at the anode and a reduced pH gradient across the system. This suggests that the two-chamber configuration may offer improved energy efficiency in certain applications. However, it is limited in output purity, producing a mixed gas stream of CO_2 (up to 80%) and O_2, which requires additional separation steps to isolate each gas for downstream use or storage. In contrast, the three-chamber electrolyzer enables more effective gas separation, potentially minimizing the need for complex post-processing. Therefore, while the two-chamber design may be more energy-efficient, it introduces greater challenges in achieving high-purity gas products.

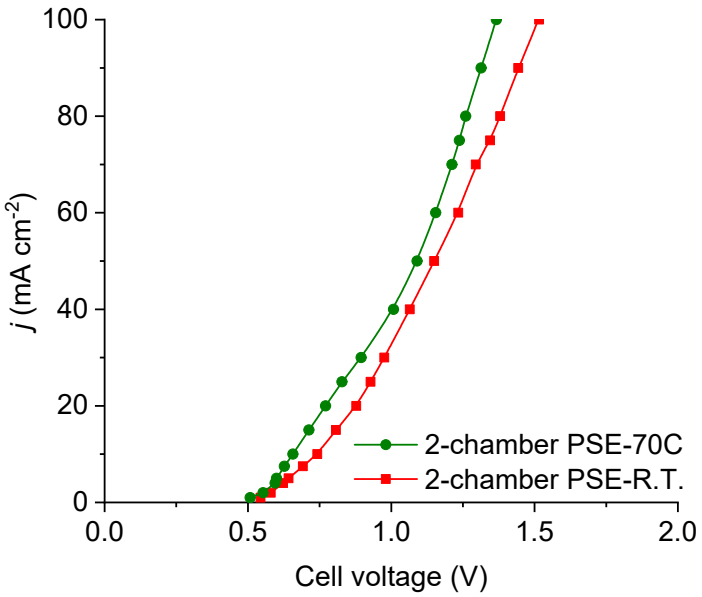

Supplementary Fig. 15. Temperature effect: Electrochemical devices for carbon capture and pure CO_2 regeneration using 2-chamber under room temperature and 70°C.

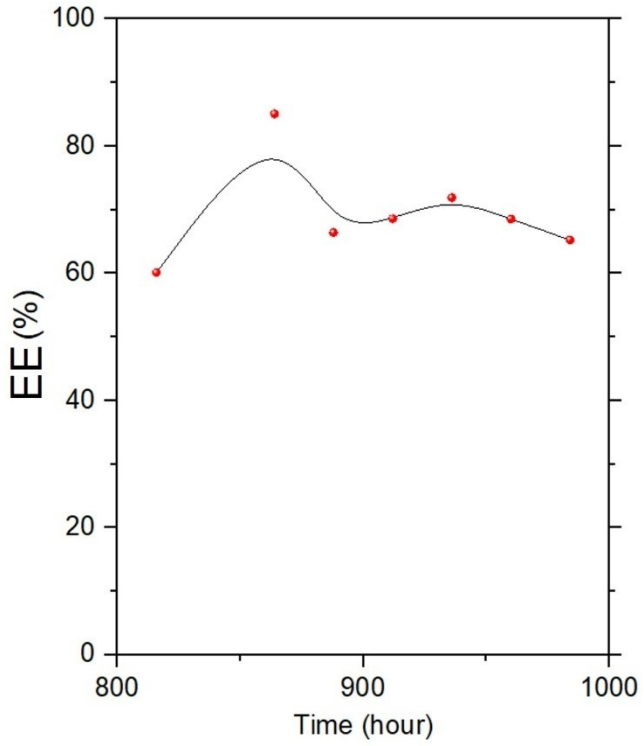

Supplementary Fig. 16. Electron efficiency of the device from 900 to 1000 hours during 1000-hour stability using simulated flue gas (3.5%) with a constant current density of 50 mA cm^{-2}.

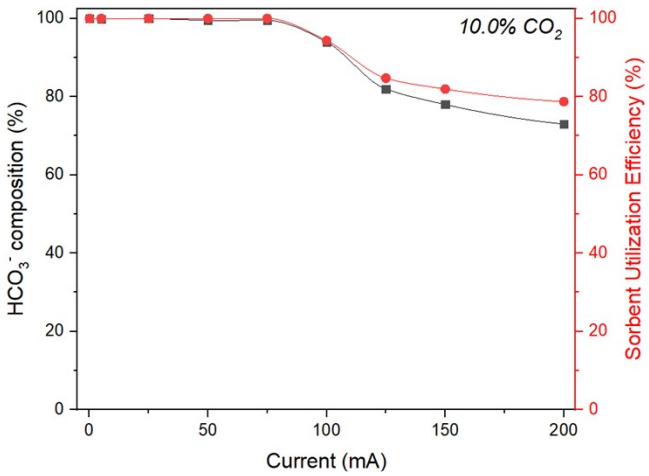

Supplementary Fig. 17. Bicarbonate composition and SUE based on titration under 10% CO_2 concentration.

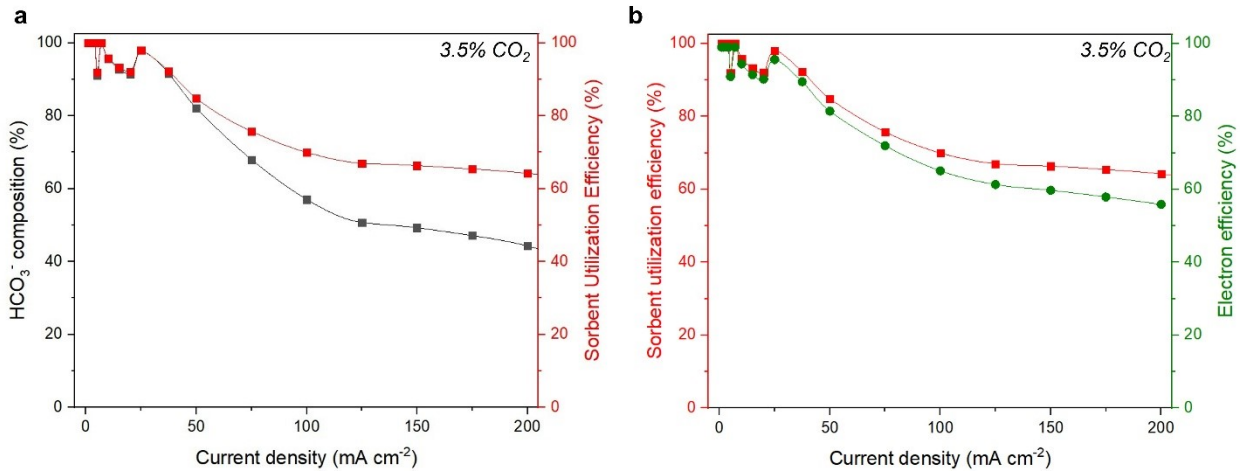

Supplementary Fig. 18. Bicarbonate composition, SUE, and EE based on titration under 3.5% CO_2 concentration

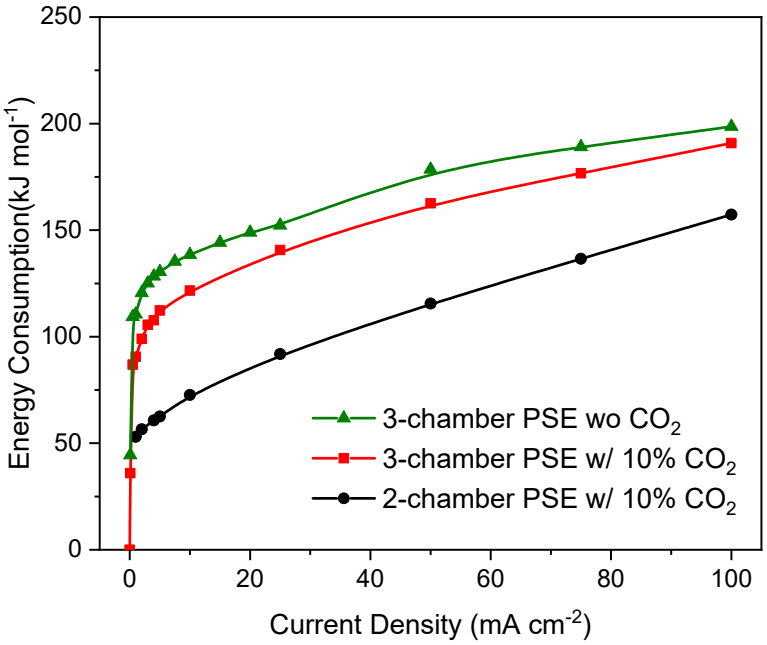

Supplementary Fig. 19. Energy consumption of the PSE electrolyzer with different chamber configurations and with/without CO_2 from 1 to 100 mA cm^{-2} (assuming similar captured efficiency, n=1, where all captured carbon species are bicarbonates). When separating CO_2 capture and regeneration, the system shows higher cell voltage (performing pure ORR) and lower transport number. While using 2-chamber PSE with CO2, the transport number is similar to that of the case of 3-chamber configuration with CO_2, but with a much lower cell voltage due to the reduced electrolyzer pH gradient.

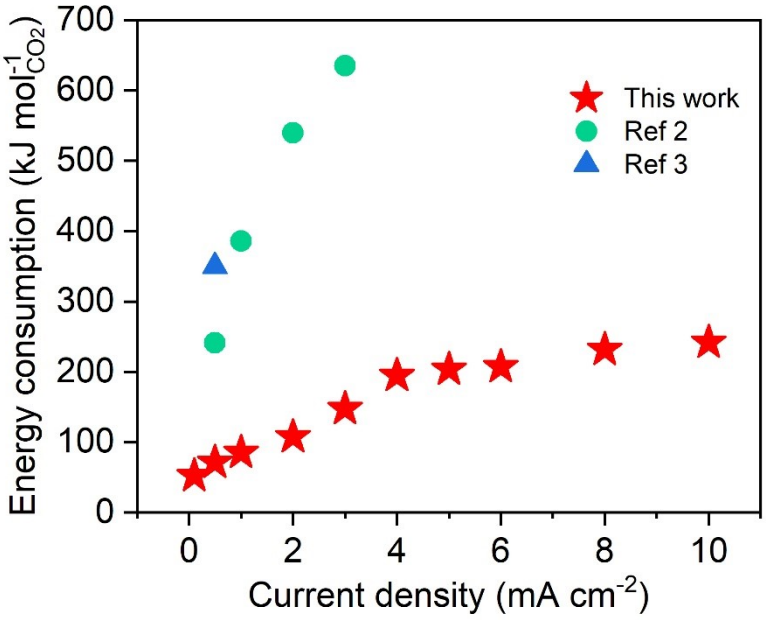

Supplementary Fig. 20. Energy consumption comparison for DAC. Key difference between our previous work (Ref 2)[4] and this work:

	Ref 2: Nature 2023[4]	**This Work (Current Manuscript)**
Energy consumption	350 kJ/mol$_{CO2}$ @ 50 mA cm^{-2}	150 kJ/mol$_{CO2}$@ 50 mA cm^{-2}, due to high absorption efficiency and EE
SUE/EE$_{CO2}$	< 50%	up to 90%, 65% for DAC at 25mA cm^{-2}
pH gradient	Very large	Can be reduced in both 2 and 3-chamber PSE
Stability	~70 h	>1000 h stable operation

(1) Mechanism: The prior system operated via a CO_3^{2-} pathway, with limited electron efficiency due to high proton demand for CO_2 release. In contrast, the present CEM-based system enables HCO_3^--mediated capture and release, improving electron utilization and reducing energy consumption. (2) The previous integrated absorption-regeneration architecture is suitable for point-source CO_2 but becomes mass-transport limited at the ppm levels relevant for DAC. Our design intentionally decouples the absorption step from regeneration, allowing large-scale DAC to use inexpensive air channel contactors with extended retention time, while the electrochemical device operates at practical current densities without gas-phase mass-transfer limitations. (3) Ion transport: Instead of transporting carbonate species, this system leverages Na^+ transport across the CEM, creating a fundamentally different electrolyte environment and enabling continuous NaOH regeneration, avoiding the use of unstable AEM. (4) Performance: The system demonstrates substantially reduced energy consumption (~150 vs ~350 kJ mol^{-1} CO_2 at comparable current density), higher efficiency, and >1000 h stability, representing a significant advancement over prior work.

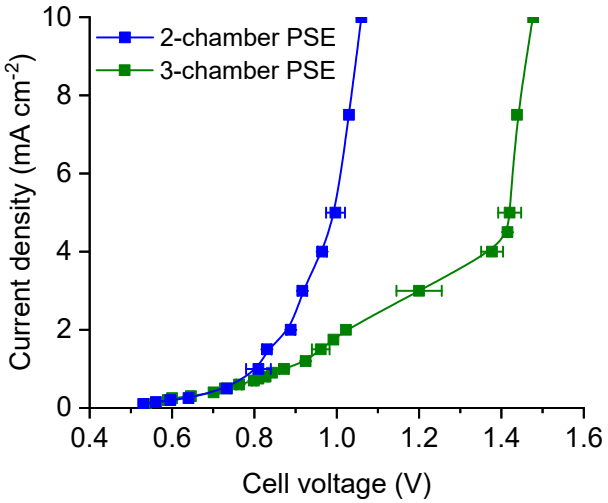

Supplementary Fig. 21. I-V curves of PSE electrolyzers for CO_2 capture from 10% CO_2 feed gas and atmospheric CO_2 under 10 mA cm^{-2}. 2-chamber design exhibits lower cell voltage, which is attributed to the increased pH at the anode and reduced pH difference. This indicates that the 2-chamber configuration may offer improved energy efficiency for certain applications due to its more stable pH gradient. However, it is important to note that the 2-chamber electrolyzer is limited in its output, producing a mixture of CO_2 (up to 80%) and O_2. This mixture necessitates additional separation processes to isolate pure CO_2 and O_2 for subsequent use or storage. In contrast, the 3-chamber electrolyzer can achieve more effective separation of gases, potentially reducing the need for extensive post-processing. Thus, while the 2-chamber design itself may be more energy-efficient, it may also require more complex downstream processing to achieve the desired purity of captured gases.

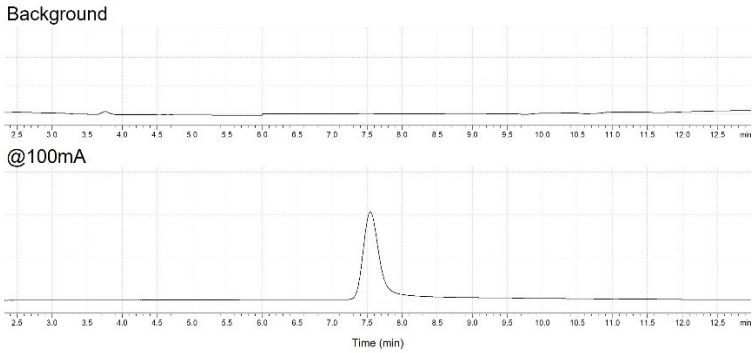

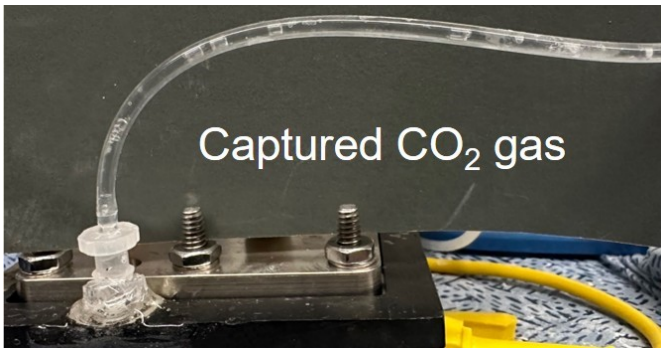

composition	background	200mA	400mA
O_2	0.132%	0.139%	0.156%
N_2	0.252%	0.273%	0.301%

Supplementary Fig. 22. Measurement of gaseous CO_2 purity captured from the middle chamber using direct air capture: The top two figures shows the FID response of the gas flow collected from the middle layer, showing an increasing CO_2 peak intensity as the reaction happens. The bottom table shows the TCD response of the collected gas flow, indicating neglectable O_2 or N_2 gas under various current densities. The O_2 and N_2 gas peaks from TCD data were used to calculate CO_2 purity, which exceeded 99.5% at both 200mA cm^{-2} and 400mA cm^{-2}.

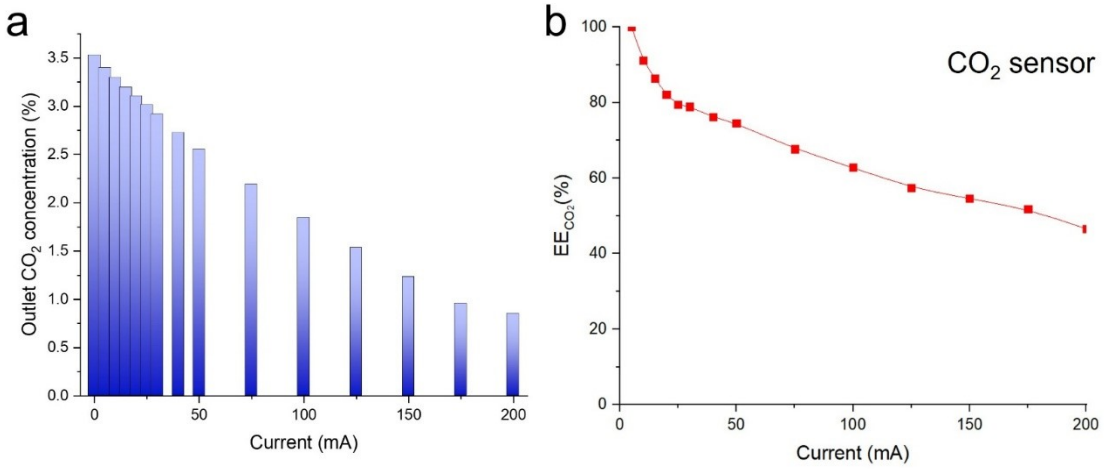

Supplementary Fig. 23. The CO_2 sensor measurements of the CO_2-lean outlet stream and EE_{CO2} under 3.5% CO_2.

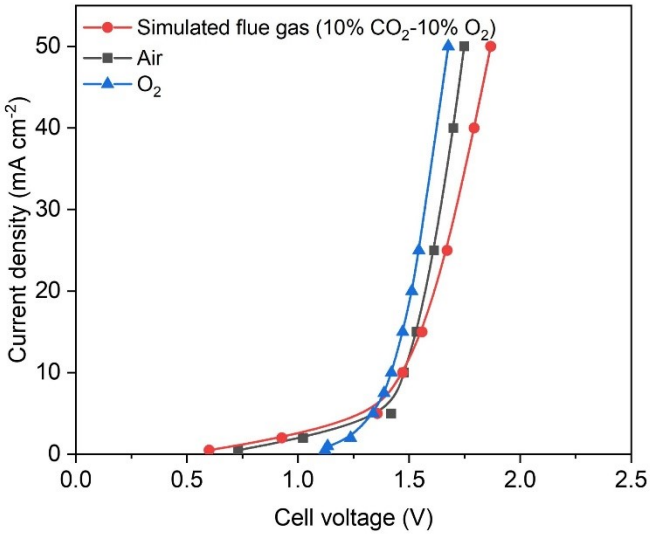

Supplementary Fig. 24. The IV-curves of 3-chamber PSE electrolyzer feeds with 10% CO_2-10% O_2-90% N_2, air and pure O_2: The onset cell voltage without buffering (pure O_2) is slightly higher than that with the buffered electrolyte (10% CO_2), indicating that the buffered environment does not introduce an additional kinetic barrier at low current densities and, in fact, reduces the pH difference and corresponding theoretical cell voltage. As the current density increases, the presence of carbonate/bicarbonate species may introduce some mass transport and kinetic limitations for ORR, resulting in a modest increase in cell voltage. To mitigate this effect, we employ a hydrophobic carbon cloth electrode to facilitate O_2 transport and minimize flooding, thereby maintaining ORR performance under these conditions.

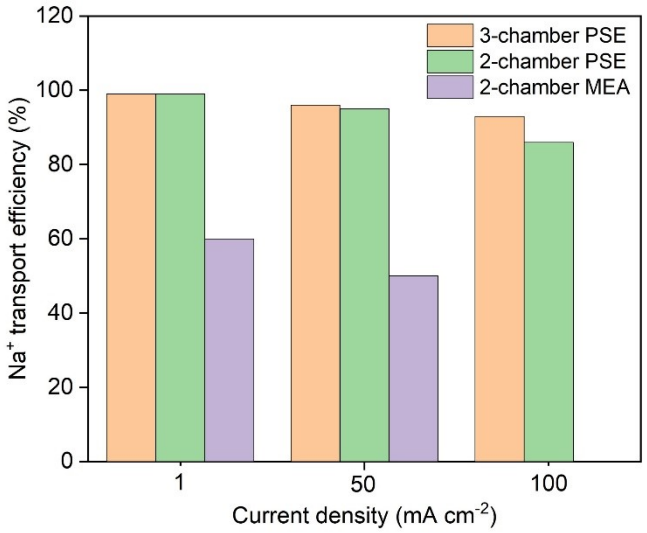

Supplementary Fig. 25. Efficiency of the 3-chamber PSE electrolyzer, the 2-chamber PSE electrolyser, and the 2-chamber MEA: In the 2-chamber MEA electrolyzer, a single membrane directly separates a strongly acidic anode environment from a strongly alkaline cathode environment. This sharp pH gradient creates a high-energy barrier for cation transport and allows a large fraction of protons to compete with Na^+, resulting in higher cell voltages and significantly reduced efficiencies.

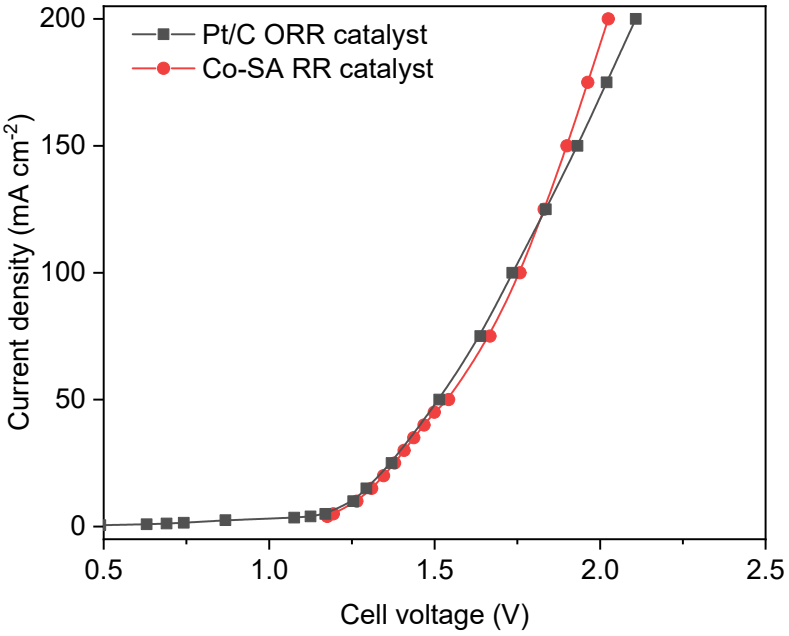

Supplementary Fig. 26. I-V curves using Noble ORR catalysts (Pt/C) and non-noble catalysts (Co-SAC).

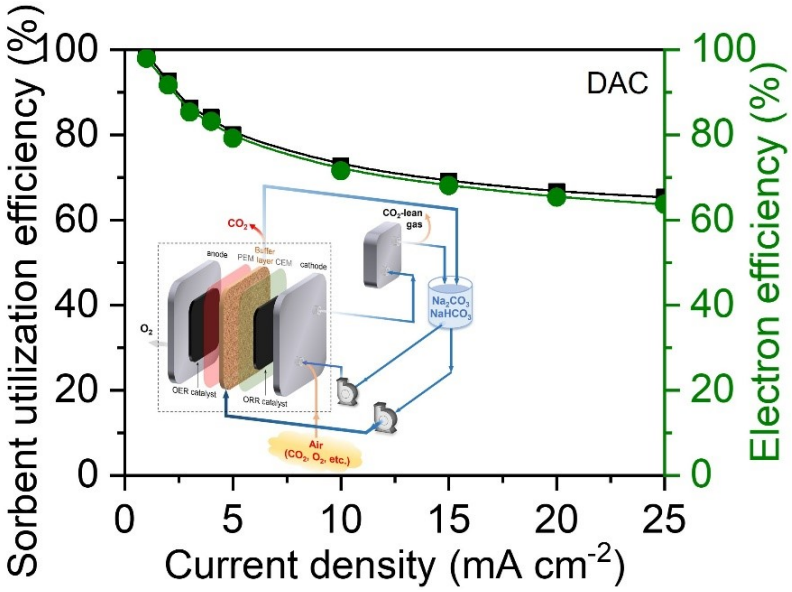

Supplementary Fig. 27. Sorbent utilization efficiency and electron efficiency for the upgraded configuration incorporating the elongated contact channel.

	Quinone-based capture	**Amine scrubbing**	**AEM electrolyzer capture**	**Calcination**	**Separated CEM electrolyzer capture**	***This work***
Temperature/°C	R.T.	120-150	R.T.	800-950	R.T.	R.T.
Energy consumption (kJ/mol)	120-300	200-400	250-500[a]	300-600	50-250	48-200[b]
O_2 tolerance	Unstable (<0.1-1% O_2, often O_2-free)	Medium[c] (3-21%)	Compatible (10-90%)	Compatible (3-21%)	Compatible (3-21%)	Compatible (10-90%)
Stability	10-50 cycles[d]	500-1500 h	<100 h	>5000 cycles	200-300 h	>1000 h
Capture rate/ capacity	3[e]	4[f]	5[g]	5[h]	5[g]	5[g]
Strong acid/ alkaline/ corrosive /organic chemicals included	2[i]	1[j]	5[k]	1[l]	2[m]	5[k]
Chemical input/waste	2[m]	1[n]	4[o]	3[p]	3[q]	4[o]
Operational complexity (e.g., evaporation, salt-dissolution)	2r	2s	5t	4u	3v	5t

Supplementary Tab. 1. Comparison of our proposed carbon capture strategy with representative methods shown in **Fig. 6e** (5 = best, 1 = worst).

[a] CO_3^{2-} as the main captured species
[b] HCO_3^- as the main captured species
[c] Absorption column itself is compatible with flue gas (3-15% O_2) or air (20% O_2), but amine oxidation and degradation
[d] Poor O_2 tolerance of absorbents
[e] 2-6 mol CO_2/kg quinone, but lower solubility than amine
[f] 1.5-2 mol CO_2/kg sorbent
[g] 11-22 mol CO_2/m^{-2} h^{-1} rate at 50 mA, 12.5-25 mol/kg NaOH
[h] 4.5-11.4mol CO_2/kg
[i] Corrosion from organic salts and quinones
[j] Use of amine
[k] acid/alkaline/corrosive/organic materials-free
[l] Use of CaO and KOH
[m] Requires organic redox molecules and supporting electrolytes, chemical degradation waste
[n] Significant chemical input, solvent loss, oxidative degradation, and waste handling
[o] Only use of noble-metal electrocatalysts and membrane, minimal sorbent consumption, and limited chemical waste.

[p] Solid sorbent cycling produces CO_2 and often requires periodic replacement
[q] Use of strong alkaline solutions
[r] Requires controlled redox cycling and solvent management
[s] Requires large absorber-stripper units and heating
[t] Integrates absorption and regeneration in one cell, eliminating thermal steps and reducing unit operations.
[u] Requires calciner, precipitator and absorption units.
[v] Requires separate absorption and regeneration units.

	Nature 2023	This Work (Current Manuscript)
Energy consumption	350 kJ/mol_{CO2} @ 50 mA cm^{-2}	150 kJ/mol_{CO2}@ 50 mA cm^{-2}, due to high absorption efficiency and EE
SUE/EE_{CO2}	< 50%	up to 90%, 65% for DAC at 25mA cm^{-2}
pH gradient	Very large	Can be reduced in both 2 and 3-chamber PSE
Stability	~70 h	>1000 h stable operation

Supplementary Tab. 2. Comparison of our previous work[4] and this work. Key differences:

1. Mechanism: The prior system operated via a CO_3^{2-} pathway, with limited electron efficiency due to high proton demand for CO_2 release. In contrast, the present CEM-based system enables HCO_3^--mediated capture and release, improving electron utilization and reducing energy consumption.

2. The previous integrated absorption-regeneration architecture is suitable for point-source CO_2 but becomes mass-transport limited at the ppm levels relevant for DAC. Our design intentionally decouples the absorption step from regeneration, allowing large-scale DAC to use inexpensive air channel contactors with extended retention time, while the electrochemical device operates at practical current densities without gas-phase mass-transfer limitations.

3. Ion transport: Instead of transporting carbonate species, this system leverages Na^+ transport across the CEM, creating a fundamentally different electrolyte environment and enabling continuous NaOH regeneration, avoiding the use of unstable AEM.

4. Performance: The system demonstrates substantially reduced energy consumption (~150 vs ~350 kJ mol^{-1} CO_2 at comparable current density), higher efficiency, and >1000 h stability, representing a significant advancement over prior work.

Reference	Current density (mA cm^{-2})	Energy consumption (kJ mol-1)
Ref [29] nc	3.3	155.4
Ref [27]	10	300
	60	320
Ref [30]	5	374
Ref [30]-optimized	5	164
Ref [31] EES	0.4	242
Ref [23]-1	1	75
	100	290
Ref [23]-2	1	50
	100	150
Ref [26]	100	380
This Work	1	48
	100	180

Supplementary Tab. 3. Comparison of this work and emerging technologies for point source capture in **Fig. 5d**: ref [23-1] corresponds to the carbonate feed, and ref [23-2] represents the bicarbonate feed, which leads to lower energy consumption. All references cited in this table are included in the main text.

Reference

1. Xia, C., Xia, Y., Zhu, P., Fan, L., and Wang, H. (2019). Direct electrosynthesis of pure aqueous H_2O_2 solutions up to 20% by weight using a solid electrolyte. Science *366*, 226-231. doi:10.1126/science.aay1844.
2. Xia, C., Zhu, P., Jiang, Q., Pan, Y., Liang, W., Stavitski, E., Alshareef, H.N., and Wang, H. (2019). Continuous production of pure liquid fuel solutions via electrocatalytic CO2 reduction using solid-electrolyte devices. Nat. Energy *4*, 776-785. 10.1038/s41560-019-0451-x.
3. Zhu, P., and Wang, H. (2021). High-purity and high-concentration liquid fuels through CO2 electroreduction. Nat. Catal. *4*, 943-951. 10.1038/s41929-021-00694-y.
4. Zhu, P., Wu, Z.-Y., Elgazzar, A., Dong, C., Wi, T.-U., Chen, F.-Y., Xia, Y., Feng, Y., Shakouri, M., Kim, J.Y., et al. (2023). Continuous Carbon Capture in An Electrochemical Solid-Electrolyte Reactor. Nature *618*, 959-966. 10.1038/s41586-023-06060-1.
5. Wu, Z.-Y., Karamad, M., Yong, X., Huang, Q., Cullen, D.A., Zhu, P., Xia, C., Xiao, Q., Shakouri, M., Chen, F.-Y., et al. (2021). Electrochemical Ammonia Synthesis via Nitrate Reduction on Fe Single Atom Catalyst. Nat. Commun. *12*, 2870. 10.1038/s41467-021-23115-x.
6. Zhang, X., Fang, Z., Zhu, P., Xia, Y., and Wang, H. (2025). Electrochemical regeneration of high-purity CO2 from (bi)carbonates in a porous solid electrolyte reactor for efficient carbon capture. Nat. Energy *10*, 55-65. 10.1038/s41560-024-01654-z.
7. Kim, J.Y.T., Zhu, P., Chen, F.-Y., Wu, Z.-Y., Cullen, D.A., and Wang, H. (2022). Recovering carbon losses in CO_2 electrolysis using a solid electrolyte reactor. Nat. Catal. *5*, 288-299. 10.1038/s41929-022-00763-w.
8. Doney, S.C., Fabry, V.J., Feely, R.A., and Kleypas, J.A. (2009). Ocean acidification: the other CO2 problem. Annual Review of Marine Science *1*, 169-192.